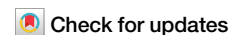# Seasonal biases in fluorescence-estimated chlorophyll-a derived from biogeochemical profiling floats

Check for updates

Jacqueline S. Long[1] ✉, Yuichiro Takeshita [1], Joshua N. Plant[1], Nina Buzby[2], Andrea J. Fassbender [3] & Ken S. Johnson [1]

Marine phytoplankton biomass and chlorophyll-a concentration are often estimated from pigment fluorescence measurements, which have become routine despite known variability in the fluorescent response for a given amount of chlorophyll-a. Here, we present a near-global, monthly climatology of chlorophyll-a fluorescence measurements from profiling floats combined with ocean color satellite estimates of chlorophyll-a concentration to illuminate seasonal biases in the fluorescent response and expand upon previously observed regional patterns in this bias. Global biases span over an order of magnitude, and can vary seasonally by a factor of 10. An independent estimate of chlorophyll-a from light attenuation shows similar global patterns in the chlorophyll-fluorescence bias when compared to biases derived from satellite estimates. Without accounting for these biases, studies or models using fluorescence-estimated chlorophyll-a will inherit the seasonal and regional biases described here.

Fluorescence spectroscopy is one of the most common methods of estimating in situ chlorophyll-a concentrations (Chl-a) in seawater[1]. Robust, scalable, off-the-shelf sensors have allowed the oceanographic community to routinely collect these measurements from ships, moorings, marine mammals, and autonomous vehicles[2]. Autonomous measurements of chlorophyll fluorescence (Chl_{FL}) have filled observation gaps in previously difficult-to-sample regions and seasons (Fig. 1, and Supplementary Fig. 1), and are increasing in global coverage through programs such as Biogeochemical (BGC)-Argo. Given the prevalence of profiling float measurements that resolve subsurface features[3,4], they have been used in a wide variety of applications, such as for estimates of primary production[5–8], carbon cycling and export[9,10], bloom phenology[11], ecosystem studies[12], biogeographical classification[13], and to assess marine health for commercial industries[14]. However, there are a variety of factors that affect the intensity of the fluorescence emission that are not related to the chlorophyll-a concentration directly: fluorescence by primary pigments other than Chl-a and accessory pigments, ambient sunlight intensity, nutrient limitation, and adaptations such as non-photochemical quenching[15–17]. These mechanisms are not accounted for in Chl_{FL} sensor calibration conversions, causing persistent spatial and temporal patterns in the ratio of Chl_{FL} to Chl-a that can lead to an order of magnitude error globally[18], reducing the full potential of this dataset[19] (e.g., Supplementary Fig. 2).

To quantify and correct biases in Chl_{FL}, independent and co-located measurements of Chl-a and Chl_{FL} can be used to calculate a multiplicative 'bias correction' (Chl_{FL}:Chl-a). This correction can be used to adjust the sensor's factory calibration, yielding unbiased Chl_{FL} estimates. The standard technique to validate Chl-a estimates is by using high-performance liquid chromatography (HPLC)[20]. A detailed analysis by Roesler et al.[18] compared measurements of Chl_{FL} from fluorometers (the primary Chl_{FL} instrument on BGC-Argo floats) and Chl-a from HPLC, and found a global median bias correction of 2. However, regional patterns in the bias correction, ranging from 1 in the Arabian Sea and Arctic Ocean to >6 in the Southern Ocean, were also identified. Regardless, a bias correction of 2 is currently applied to all BGC-Argo Chl_{FL} data during the quality control process[21]. While this improves the global average, systematic regional biases still persist. Further, these bias corrections are expected to vary seasonally in some regions, as phytoplankton groups shift[22], or limiting nutrients, such as iron, become available[23]. Due to the sparseness of co-located HPLC and Chl_{FL} measurements, many ocean regions were not evaluated by Roesler et al.[18], and their associated correction factors remain unconstrained, limiting our ability to accurately adjust the global float Chl_{FL} dataset. As BGC-Argo float coverage increases, a spatially and temporally resolved bias correction is desired.

Estimates of Chl-a from satellites (Chl_{SAT}) and light attenuation (K_d) measured using radiometers on profiling floats (Chl_{Kd})[24] present alternative

[1]Monterey Bay Aquarium Research Institute, 7700 Sandholdt Rd., Moss Landing, Seattle, CA, USA. [2]University of Washington, School of Oceanography, 1410 NE Campus Pkwy, Seattle, WA, USA. [3]NOAA Pacific Marine Environmental Laboratory, 7600 Sand Point Way NE, Seattle, WA, USA. ✉ e-mail: jacki@submarine.earth

means for quantifying bias corrections in more ocean regions and at more frequent time intervals than HPLC Chl-a measurements. Chl_{SAT} and Chl_{Kd} estimates are based on empirical relationships between optical measurements and Chl-a derived from HPLC measurements[25–27] and include their own uncertainties. The benefit of using Chl_{SAT} to derive bias corrections is the near-daily global coverage of observations that span the full BGC-Argo float record, making it possible to better resolve regional patterns and seasonality in the Chl_{FL} bias. Using the Chl_{Kd} approach requires the co-deployment of a chlorophyll fluorometer with a radiometer, which is presently the case for <35% of fluorometer-equipped BGC-Argo floats, limiting its spatiotemporal coverage.

Here, we present a near-global, 5° × 5° gridded monthly climatology of bias corrections derived from spatiotemporal matchups of Chl_{FL} float profiles and Chl_{SAT}, including 631 floats and 45,318 profiles between 2008 and 2023 (Fig. 1). The same analysis was conducted using Chl_{Kd} for the subset of floats that carried radiometers, including 228 floats and 16,754 profiles. We find coherent spatial and seasonal biases in both the Chl_{SAT} and Chl_{Kd} bias corrections, broadly consistent with previous HPLC-based corrections[18]. However, a systematic discrepancy of ~35% was observed between Chl_{SAT} and Chl_{Kd}, and should be a focus of future research to resolve the differences. Our climatology product can be used to apply seasonally resolved educated uncertainties to open ocean Chl_{FL} measurements

made with SeaBird (previously WET Labs) ECO and MCOMS sensors from any platform.

Results and discussion
Regional variability
The satellite-based climatology of annual median bias corrections (Fig. 2g) exhibits clear spatial patterns. Excluding the equatorial Pacific, the low latitudes and subtropical gyres have low bias corrections, with Chl_{FL} underestimated relative to Chl_{SAT} (values < 1) in some areas. The annual climatological bias correction increases towards higher latitudes, reaching more than 10 in latitudes below −52° of the Southern Ocean. While there is limited coverage in the Indian Ocean, climatological values are low in observed regions. These global patterns are similar to those found by Roesler et al.[18], and previous works have explored the underlying mechanisms responsible for the spatial variations. This variability is partially attributed to changing phytoplankton species and community composition[18], as different phytoplankton species contain distinct photopigments, having unique fluorescence and absorption spectra[22]. This may contribute to the bias correction variability from low to high latitudes as dominant phytoplankton species change. Cell size has also been shown to affect the fluorescence to Chl-a ratio[22], further explaining the general latitudinal trend, as phytoplankton size tends to shift with latitude. Additionally, it has been well documented that the fluorescence to Chl-a ratio increases when phytoplankton is iron-limited, and nitrate is replete[23,28–30]. In alignment with these studies, we find that regions exhibiting the largest required bias corrections, such as the subarctic Pacific and Atlantic, equatorial eastern Pacific, and the Southern Ocean, are also known to be high-nutrient-low-chlorophyll zones, and iron-limited[31,32]. However, it is possible that other factors, such as phytoplankton cell size and community shifts, are contributing to the high biases found in these regions[33,34].

The area-weighted, global median bias correction based on satellite-float matchups was 3.6; higher than the global average of 2 reported by Roesler et al.[18]. Differences could be due to a variety of factors. First, the bias corrections by Roesler et al.[18] were derived from direct comparisons of Chl_{FL} to Chl-a from HPLC analysis, whereas ours were derived from matchups with 8-day averaged satellite measurements, as explained in the "Methods" section. Second, the spatial coverage between the two studies differs substantially. The dataset included in Roesler et al.[18] was largely limited to the Mediterranean and Atlantic Oceans, with <20 floats in the Southern Ocean and 3 floats in the Pacific. At that time, no data were available from the North Pacific, the Pacific sector of the Southern Ocean, or the Indian Ocean.
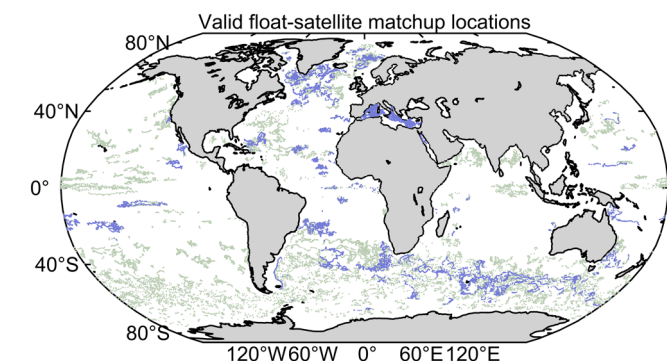

Fig. 1 | Locations of float data used in the study between 2008 and 2023. BGC-Argo float profile locations of float fluorescence-estimated chlorophyll-a only (Chl_{FL}, green) from 631 floats and 45,318 profiles, and both Chl_{FL} and irradiance-estimated chlorophyll-a (Chl_{Kd}, purple) from 228 floats and 16,754 profiles.
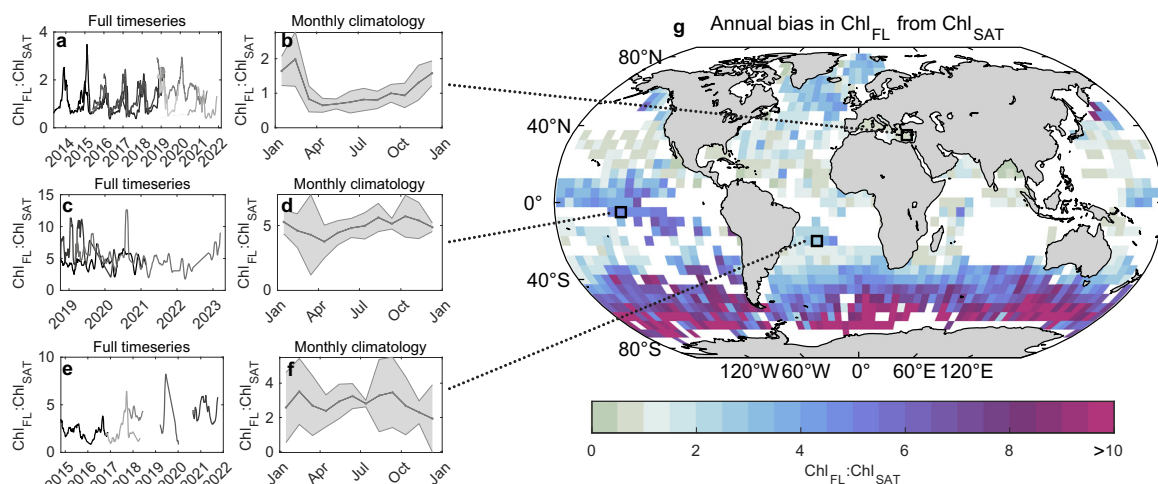

Fig. 2 | Regional and temporal variability in Chl_{FL} bias estimated from Chl_{SAT}. **g** Global distribution of annual climatological biases (calculated as the median of monthly climatological values at each 5° × 5° grid). **b, d, f** Climatologies of monthly medians for three selected regions with the interannual spread (1-sigma) shaded in gray. **a, c, e** Full-time series of Chl_{FL} to Chl_{SAT} ratios for each region are shown with gray shades representing unique floats. A moving mean filter (MATLAB, movmean) of 30 days was applied to daily interpolated data to smooth higher-frequency variations and more clearly visualize seasonal cycles.
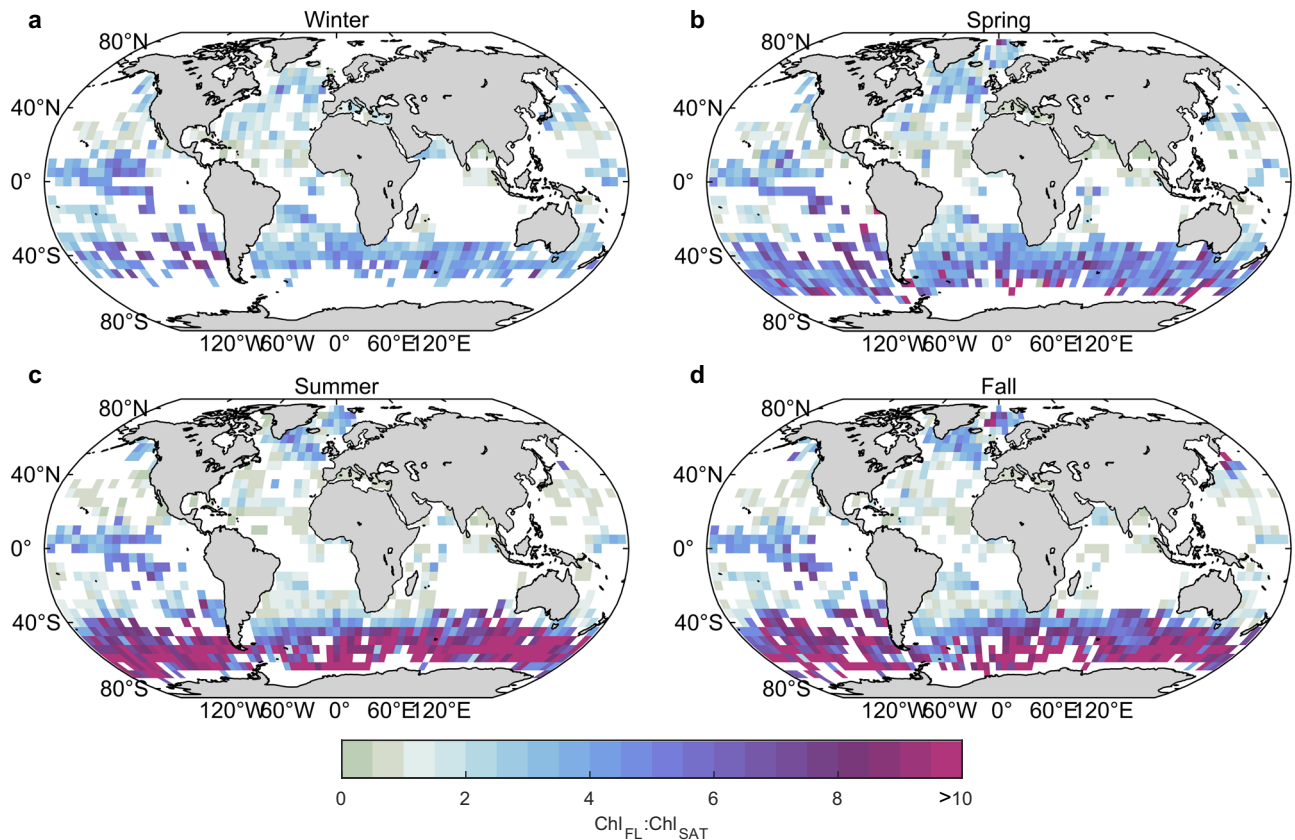
Fig. 3 | Seasonal variability in Chl$_{FL}$ biases estimated from Chl$_{SAT}$. Grids in the northern and southern hemispheres were split to show the same season for each global image for **a** winter, **b** spring, **c** summer, and **d** fall.

Though they attempted to account for spatial gaps in their dataset, it is likely that reported global estimates were biased towards regions with direct observations. It is also likely that the global median bias correction presented here will change as gaps in the existing dataset, such as the North Pacific and the Indian Ocean, become populated with BGC-Argo floats. Still, this serves as a valuable comparison against Roesler's global estimate, as both studies conclude that Chl$_{FL}$ overestimates Chl-a globally by several factors. However, it is also clear that a single global bias correction is insufficient[23,35,36], and regionally and temporally resolved bias corrections are required to obtain accurate Chl-a estimates from in situ Chl$_{FL}$ measurements across the globe.

Seasonal variability

There were clear, global patterns in the seasonal cycle of the bias corrections (Fig. 3), demonstrating that applying a monthly-to-seasonally resolved bias correction to Chl$_{FL}$ can further improve estimates of Chl-a derived from Chl$_{FL}$. The bias correction changed by more than an order of magnitude over the annual cycle in some regions (Fig. 4). Seasonal biases could be classified into the following three categories: (1) having a seasonal cycle with minimal interannual variability (Fig. 2a, b), (2) having a seasonal cycle with significant interannual variability (in phasing and/or magnitude; Fig. 2e, f), and (3) having no obvious seasonal cycle (Fig. 2c, d). As more data become available, it may be possible to assign a category to each grid and provide specific recommendations for bias correction. For the first case, we advise using the monthly climatological bias correction in order to accurately calculate Chl-a throughout the year. In regions with large interannual variability in the seasonal cycle, a static monthly climatological bias correction may not fully remove seasonal biases in each year. In these regions, it may be necessary to conduct float-satellite matchups for the target month and year. Due to limited data availability, the magnitude of interannual variability is unclear in many regions, however it may be expected to have a
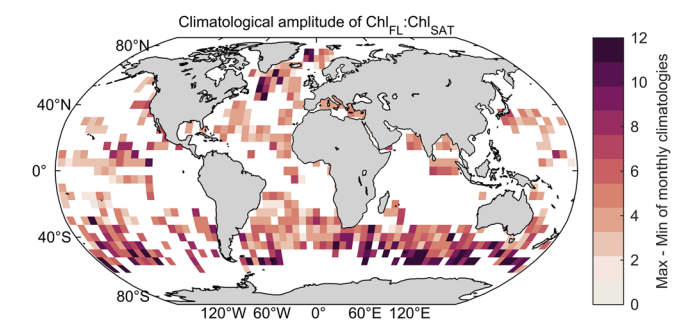

Fig. 4 | Global patterns of seasonal amplitude in Chl$_{FL}$ bias estimated from Chl$_{SAT}$. Calculated as the maximum−minimum of monthly climatological bias values in each 5° × 5° grid with data for at least 7 months of the climatology.

dominant effect in highly dynamic regions, such as frontal zones. If no clear seasonal cycle exists, or in data-limited regions where a monthly climatology has not yet been accurately resolved, applying the climatological annual median value is advised.

The highest seasonal cycle amplitudes for the bias correction were observed in the northwestern Atlantic and Southern Ocean (Fig. 4), where seasonal amplitudes exceeded 10 in some regions. Seasonal peaks occurred in the summer and fall throughout most of the Southern Ocean and Subpolar North Atlantic (Supplementary Fig. 3), with minimums in the winter, consistent with prior observations[37]. Seasonality in the bias correction likely reflects changes in phytoplankton community structure, nutrient availability, and ambient light intensity associated with seasonal mixed layer dynamics.
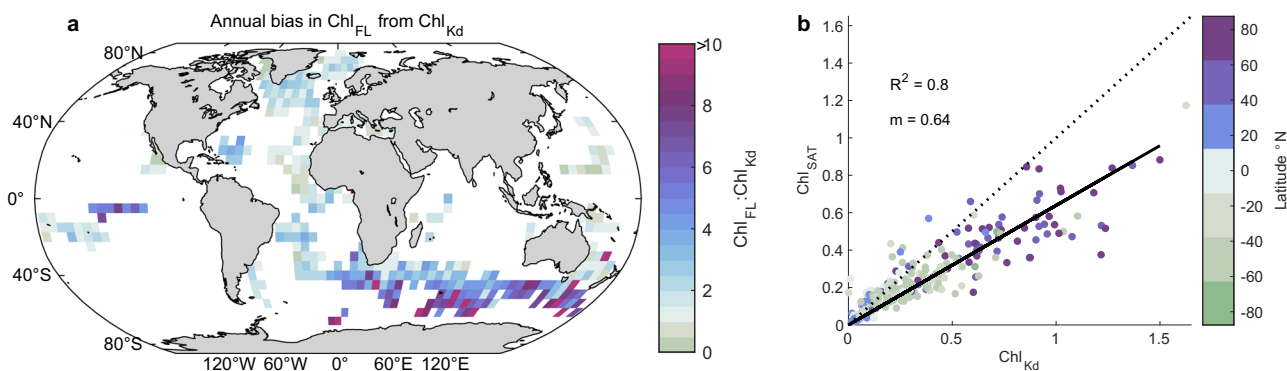
Fig. 5 | Chl_{Kd} estimates compared to Chl_{FL} and Chl_{SAT}. a Global variability in the annual climatology of Chl_{FL} bias estimated from Chl_{Kd}. **b** Chl_{SAT} versus Chl_{Kd} based on the gridded values used to create the map in Supplementary Fig. 5, showing overall agreement between the two methods. Markers are colored by the centered latitude value of each grid.

Comparison of satellite and radiometric chlorophyll-a estimates

Radiometric estimates of Chl_{Kd} on BGC-Argo floats are a promising option for calculating bias corrections (see the "Methods" section). They are frequently co-located with Chl_{FL} measurements and provide an independent estimate of Chl-a using light attenuation, and they gather data below the first optical depth. While these sensors were not historically common on BGC-Argo floats, they are now becoming more common on floats, with growing global coverage (Fig. 1). Annual climatologies for the K_d and satellite-based bias corrections exhibit strong agreement in terms of the spatial pattern (Figs. 5a and 2g), with higher seasonal amplitudes in $Chl_{FL}:Chl_{Kd}$ observed in the Equatorial Pacific (Supplementary Fig. 4). Low bias corrections were observed at low latitudes, and higher biases were observed in the Southern Ocean, Subpolar North Atlantic, and Equatorial Pacific.

Chl_{SAT} estimates were ~36% lower than Chl_{Kd}, based on matchups between satellite observations and floats equipped with radiometers (Fig. 5b, $R^2 = 0.8$). This would lead to an underestimation of Chl-a if the satellite-based bias corrections were implemented relative to the K_d-based approach. This offset may be driven by larger biases in high latitude regions compared to the subtropics and equatorial waters (Supplementary Fig. 5); regions where the Chl_{Kd} and Chl_{SAT} algorithms used herein are poorly constrained[25–27]. It is outside the scope of this project to determine whether Chl_{SAT} or Chl_{Kd} is more accurate, but this should be examined closely in future studies, including the effect of decreasing sun angles on radiometer-estimated K_d. Nonetheless, similarities in the climatological spatial and seasonal patterns between the two methods suggest that both methods agree on the presence of large-scale spatiotemporal variability in the Chl_{FL} bias.

Considerations

While the satellite-based bias corrections presented in this study can be used to improve estimates of Chl_{FL} globally, there are several limitations worth noting. First, the bias correction is derived by comparing satellite and float measurements over the first optical depth, which ranges from about 5–45 m globally. As a result, these bias corrections reflect the influences of phytoplankton community structure and physiology in the near-surface waters[22]. In cases when the seasonal mixed layer is shallower than the first optical depth (the depth horizon of this study), a mix of phytoplankton groups living above and below the mixed layer may necessitate the application of different bias corrections seasonally. Previous studies have demonstrated that bias corrections can vary with depth, as phytoplankton communities change and experience changes in ambient light and/or nutrient availability[22,38,39]. Thus, there may remain a depth dependence to biases in Chl_{FL}, even after applying the satellite or light attenuation-based bias correction[24]. As subsurface production and phytoplankton biomass have been shown to play an important role in carbon export[40], depth-resolved bias corrections are needed to obtain accurate subsurface biomass[3] and productivity rates[41]. Additionally, the effect of non-photochemical

quenching (NPQ, a suppression in fluorescence where light energy is instead dissipated as heat) is present in the first optical depth. Corrections were applied to day-time data for NPQ, and results were similar whether using corrected daytime or nighttime data (see discussion in "Methods" section), however unconstrained NPQ corrections may account for some regional variability (e.g., the Equatorial Eastern Pacific, Supplementary Fig. 6), especially for regions with regularly shallow mixed layers or mixed layers impinging on signals of deep fluorescence maxima[42].

Second, seasonal errors in Chl_{SAT} or Chl_{Kd} could contribute to the seasonal variations in the reported bias corrections[43]. However, we believe that this effect is not the dominant driver of observed seasonal patterns in the bias corrections. Seasonal biases in $Chl_{FL}:Chl$-a have been observed using other methods of Chl-a estimation[22], including extracted Chl-a measurements[7]. Furthermore, it is reasonable to expect that Chl_{SAT} and Chl_{Kd} estimates perform better in regions where in situ data were available for their algorithm development[44], and thus different algorithms to compute Chl_{Kd} or Chl_{SAT} could work better in certain regions than others[23,45].

Third, we have used a static boundary of $5° \times 5°$ lat/lon grids for this product. However, the driving forces behind the spatiotemporal patterns in the bias corrections are inherently dynamic and could occur at smaller spatial scales. As a result, different water masses may occupy a single grid, especially in regions with dynamic fronts, such as the Southern Ocean, where sharp gradients in surface nitrate and phytoplankton communities exist[46]. A water mass framework could be implemented if, for example, bias factors were determined according to environmental characteristics[47].

Finally, spatiotemporal patterns in the bias corrections reported here will likely apply to Chl_{FL} measurements made from any platform due to the physiological nature of the fluorescence response. However, it is important to note that the bias corrections reported in this paper apply to the Seabird (previously WET Labs) ECO and MCOMS sensor products, and magnitudes may vary for other manufacturers depending on their calibration protocols.

Conclusions

Our study provides a comprehensive, near-global, monthly climatology of the bias in fluorescence-estimated chlorophyll-a that we derive from spatiotemporal matchups of Chl_{FL} float profiles and chlorophyll-a estimates from satellite and radiometric observations. The patterns of bias corrections were consistent across both methods, however there was a systematic discrepancy between satellite- and radiometer-based Chl-a estimates that warrants further investigation. By quantifying seasonal and regional biases in Chl_{FL} estimates, our findings underscore the importance of accounting for these biases to obtain accurate assessments of Chl-a concentrations in the ocean. The observed spatial patterns in bias corrections spanned over an order of magnitude and were highest in iron-limited regions. Seasonal variability in bias corrections changed by an order of magnitude over the

annual cycle in some regions. These patterns of variability emphasize the complex interplay between phytoplankton physiology, community composition, nutrient availability, phytoplankton size classes, and environmental conditions, highlighting the necessity for a space and time-resolved bias correction approach.

Moving forward, an increased number of radiometers co-deployed with Chl-a fluorometers will help to improve bias correction estimates. Spatiotemporal discrepancies can be minimized using the Chl_{Kd} approach compared to Chl_{SAT} because the fluorescence and downwelling irradiance measurements are made simultaneously. Furthermore, downwelling irradiance data can be used to implement a more robust NPQ correction[48], reducing uncertainty in day-time Chl_{FL} estimates (Supplementary Fig. 6). Finally, bias corrections could be computed from machine learning approaches by combining satellite observations and other biogeochemical variables measured on floats, such as nitrate and downwelling irradiance[49]. Anticipated increases in the number of floats equipped with radiometers in the coming years will improve our ability to quantify ocean productivity in near-real time and to monitor the health of ocean ecosystems. These methods of correction are currently being explored by the Argo community for application in delayed-mode quality control procedures. It is recommended that users of Chl_{FL} data, especially those combining Chl_{SAT} and Chl_{FL}, apply the results from this study as an educated uncertainty when interpreting Chl_{FL} data.

Methods
Float data
Synthetic profile files were downloaded from the Argo Global Data Assembly Center (2023–05 snapshot, doi:10.17882/42182). There were 631 floats equipped with Seabird Scientific chlorophyll fluorescence sensors from 2 April 2008 to 9 May 2023 (Fig. 1), with 503 ECO sensors, and 128 MCOMS sensors. All floats carried conductivity-temperature-depth sensors, and a subset of floats ($n = 228$) carried downwelling radiometer sensors (Seabird Scientific OCR-504) that included measured radiance at 490 nm (Fig. 1). Profiling float data go through post-deployment quality control following standard Argo protocols[21,50]. For Chl_{FL} data, the field CHLA_ADJUSTED represents Chl_{FL} data that has gone through the QC process, and the CHLA field represents raw Chl_{FL} based on applying factory calibration coefficients in mg m^{-3}. For ECO and MCOMS sensors, the dark counts are subtracted from the raw sensor counts and then converted to CHLA in mg m^{-3} by applying a factory-determined scale factor. The scale factor converts fluorescence to Chl-a concentration based on a single calibration with a monospecific culture of the diatom *Thalassiosira weisflogii*. During the QC process, four main adjustments are applied to CHLA[21]: determination of in situ dark counts based on minimum sensor counts for profiles deeper than 900 m, non-photochemical quenching correction during the day, manual inspection and flagging of bad and questionable data, and a bias correction of two[18]. The CHLA_ADJUSTED field should have these adjustments applied, but there are small inconsistencies in the details of how these adjustments are implemented, particularly for the in situ dark count and NPQ corrections. Therefore, to eliminate this source of uncertainty, we have applied the dark and NPQ correction[42] using the CHLA field for all of the floats and omitted the global bias correction of 2. However, to take advantage of the manual inspections that flagged bad data, data quality flags were imported from CHLA_ADJUSTED of 1, 5, and 8, which correspond to good data, value changed, and estimated value. Data with a quality flag of 2 ("probably good") were not included in order to avoid unknown uncertainties from using these flagged data. The latter two flags are applied for NPQ corrected and interpolated data, respectively.

Briefly, for each float, an in situ dark correction was applied by subtracting the median of the minimum Chl_{FL} value of the first five deep (>900 m) profiles from all data[23]. Floats that were recently deployed and did not collect at least five deep profiles were not included. Daytime profiles (defined as having a sun angle >0 using MATLAB function SolarAzElq) were adjusted for non-photochemical quenching[42]. This correction finds the maximum Chl_{FL} value above the mixed layer depth (defined as a density

change greater than 0.03 kg m^{-3} from a surface reference value[51]), and copies that value from its coinciding depth to the surface. Chl_{FL} values > 50 mg m^{-3} and less than 0.014 mg m^{-3} were removed from the dataset. 50 mg m^{-3} is a reasonable upper limit for open ocean chlorophyll-a maxima, whereas the lower limit is twice the factory-specified sensitivity of 0.007 mg m^{-3}. This limit of detection was confirmed in situ by looking at the smallest change between samples in the mixed layer depth of night-time profiles of floats (WMO ID's 5906514, 5904655, 5906529, 5904172) in a low chlorophyll region near Hawaii. To compare float Chl_{FL} to Chl_{SAT}, the median value of Chl_{FL} was calculated over the first optical depth (OD) because this is roughly equivalent to the depth of ocean color satellite retrievals. The first optical depth was estimated per profile as the inverse of $K_d(490)$, estimated using Chl_{SAT} using the following equations (Morel et al., Eq. (8))[25],

$$K_d(490) = 0.0166 + 0.077298 \times Chl_{SAT}{}^{0.67155} \quad (1)$$

$$OD = \frac{1}{K_d(490)} \quad (2)$$

Float temperature and salinity data were used to calculate the mixed layer depth. For this, adjusted temperature, pressure, and salinity data with Argo quality flags 1, 2, 5, and 8 were used when available. If only unadjusted data were available, quality-control flags 1, 2, 3, 5, and 8 were used. Quality control flags 1, 2, 3, 5, and 8 were used for downwelling irradiance data. A visual inspection of the irradiance data was used in Ocean Data View to remove floats and profiles with obviously bad irradiance data.

Chl_{Kd}
Chl_{Kd}, the estimate of Chl-a concentration based on the attenuation of light, was estimated from radiometric measurements of light irradiance at 490 nm[24], using the subset of floats carrying both a radiometer and fluorometer. Only the irradiance data to the first optical depth were used, rather than a threshold depth of minimum light, in order to be consistent with Chl_{SAT} and the median surface Chl_{FL} used for the study. We found that setting the integration depth to the first optical depth versus the mixed layer depth affected the final bias correction values (Supplementary Fig. 7), suggesting that this is an important definition for similar analyses. Only profiles with a sun angle >30° above the horizon were used to estimate Chl_{Kd}. A 7-point median filter was applied to each profile to minimize the effects of wave focusing at the surface, passing clouds, or changes in the float's position with respect to vertical. The 7-point median filter was chosen based on the higher sampling resolution of floats in the surface waters, for example, floats sampling at 0.2 dbar resolution would result in 1.4 m bins. The attenuation coefficient was determined from the Model 1 regression slope of depth versus the natural log of irradiance down to the first optical depth. Chl_{Kd} was estimated by inverting Eq. (8) from Morel et al.[25]. to solve for chlorophyll-a. This chlorophyll-a estimate represents a water column average between the surface and the first optical depth. Profiles with $K_d(490) < 0.0166$ (the attenuation due to water) were excluded and only profiles with an R^2 fit >80%, and a relative standard deviation of the estimated slope <10% were used to estimate Chl_{Kd}.

Satellite data
Ocean color products derived from the Moderate Resolution Imaging Spectroradiometer (MODIS) aboard the NASA Aqua satellite were used for this analysis. The level-3, 8-day averaged, 9 km resolution Chl_{SAT} concentration product (OCI algorithm[26,27]) was downloaded from the NASA Ocean Biology Processing Group. The 8-day averaged product was chosen to improve spatial coverage of the satellite data, which can be limited in daily satellite observations due to incomplete global satellite coverage, high sun glint, clouds, as well as the infrequency of same-day float-satellite matchups. Chl_{SAT} data less than 0.05 mg m^{-3} were removed based on the minimum value of in situ Chl-a data used in algorithm development[26,27].

For each float profile, Chl_{SAT} data that were within 8 km and closest in time based on the median satellite data were matched. The 8 km threshold

was chosen based on an autocorrelation threshold analysis over one year of 4 km (highest level-3 spatial resolution) MODIS Chl (1 January 2020 to 31 December 2020). Globally, this 8 km threshold corresponds to 75% or higher autocorrelation for 99.97% and 96.59% of valid matchups across longitude and latitude, respectively (Supplementary Fig. 8). The autocorrelation threshold analysis was completed separately for both the zonal and meridional directions based on similar methods[52]. Briefly, each line of latitude or longitude was treated as a discrete data series, for which an autocorrelation function can be calculated (done using MATLAB function autocorr), and defining a length scale at lag $m_{\geq 0.75}$. This lag indicates the first location within the data series at which the resulting autocorrelation coefficient is ≤0.75. The median of all spatiotemporally matched satellite data per profile was used to compare to the float data.

Building the climatology

The ratio of Chl_{FL} data to the median of Chl_{SAT} matchups or Chl_{Kd} were taken per profile, and represent the final data used to estimate climatological correction factors, where Chl_{FL} and Chl_{Kd} are median values taken within the first optical depth. Within a $5° \times 5°$ gridded area, the median of Chl_{FL}:Chl_{SAT} or Chl_{FL}:Chl_{Kd} data for a single month, year, and float are taken first, then the median of this data across floats for a month and year, and finally, the median and standard deviation across all years for a month is taken, producing the final gridded climatological median and standard deviation values presented here. Seasonal climatological values are taken as the median of monthly climatological values for the northern/southern hemispheres, respectively, for December, January, February (winter/summer), March, April, May (spring/fall), June, July, August (summer/winter), September, October, November (fall/spring). Amplitudes were calculated as the absolute difference between the maximum and minimum monthly climatological values for each $5° \times 5°$ grid with more than 6 months of valid data, and the negative inverse of bias corrections <1 was taken prior to calculating amplitudes. Area-weighted values are reported for calculated global medians. For all variable-variable plots and corresponding linear fit statistics, outliers were removed using Chauvenet's criterion. The mean of the monthly Chl_{FL}:Chl_{SAT} standard errors (SE) for each grid shows little regional variability (Supplementary Fig. 9, left). To gauge the significance of seasonal amplitudes, an uncertainty (U) was estimated as

$$U = \sqrt{2 \times SE^2 + 2 \times SE^2} \qquad (3)$$

Most regions were found to have a seasonal amplitude larger than the uncertainty (Supplementary Fig. 9, right), which may arise from either a well-defined seasonal shape or large month-to-month variability with no clear seasonal shape.

The climatology presented here includes both daytime and nighttime float data. To limit potential errors introduced by the NPQ correction, it would be preferable to use only night-time profiles of Chl_{FL}, however this would have greatly reduced our number of valid Chl_{FL} profiles by ~75%, and removed the comparison to Chl_{Kd}, which is only valid during daylight hours. A linear trend between the annual gridded climatology using night-only and daytime-only profiles showed good agreement with minimal additional bias ($R^2 = 0.6$, $m = 0.9$) (Supplementary Fig. 6). To illuminate potential regional discrepancies between day and night-time data, the difference between the two was taken for the annual climatological mapped data (Supplementary Fig. 6). In general, regions showed no consistent or unique differences when using one data set versus the other, with the exception of the Eastern Equatorial Pacific where bias corrections would be lower if using daytime data compared to night time data. Uncertainties in our results of Chl_{FL} to Chl_{SAT} from float observations arise from the NPQ correction (10%, based on the slope in daytime versus night time data in Supplementary Fig. 6), spatial variability in float-satellite match-ups (25%, based on the chosen autocorrelation threshold of 75%, Supplementary Fig. 8), and the fluorescence sensor (the reported factory calibration uncertainty is 1%, however to be conservative we have chosen 5%). These result in a combined uncertainty of 27%, which is largely driven by the

autocorrelation threshold. Because it is reasonable to assume that much of the data matchups are below this threshold, we consider this uncertainty to be conservative.

Data availability

The profiling float data used in this study were obtained in May 2023 by downloading all Argo synthetic profile files directly from the Argo Global Data Assembly Center from the May 2023 snapshot (https://www.seanoe.org/data/00311/42182/). 8-day satellite data were downloaded from https://oceancolor.gsfc.nasa.gov/l3/order/. The synthetic profile files for floats were then merged into one file containing float-averaged data within the first optical depth and cross-over satellite Chl-a data for each profile, used to generate the climatologies presented in the study. Our data have been shared on Zenodo (https://doi.org/10.5281/zenodo.13137041).

Code availability

Relevant code for this study is archived in a GitHub repository under https://github.com/CarbonLab/global-fluorescence-bias/.

References

1. Holm-Hansen, O., Lorenzen, C. J., Holmes, R. W. & Strickland, J. D. H. Fluorometric determination of chlorophyll. *ICES J. Mar. Sci.* **30**, 3–15 (1965).
2. Lorenzen, C. J. A method for the continuous measurement of in vivo chlorophyll concentration. *Deep Sea Res. Oceanogr. Abstr.* **13**, 223–227 (1966).
3. Cornec, M. et al. Deep chlorophyll maxima in the global ocean: occurrences, drivers and characteristics global biogeochemical cycles. *Global Biogeochem. Cycles* **35**, 1–30 (2021).
4. Briggs, N., Dall'Olmo, G. & Claustre, H. Major role of particle fragmentation in regulating biological sequestration of CO_2 by the oceans. *Science (80-.).* **367**, 791–793 (2020).
5. Estapa, M. L., Feen, M. L. & Breves, E. Direct observations of biological carbon export from profiling floats in the subtropical North Atlantic. *Global Biogeochem. Cycles* **33**, 282–300 (2019).
6. Yang, B. et al. In-situ estimates of net primary production in the Western North Atlantic with Argo profiling floats. *J. Geophys. Res. Biogeosci.* 1–16 https://doi.org/10.1029/2020jg006116 (2021).
7. Long, J. S., Fassbender, A. J. & Estapa, M. L. Depth-resolved net primary production in the Northeast Pacific Ocean: a comparison of satellite and profiling float estimates in the context of two marine heatwaves. *Geophys. Res. Lett.* 1–11 https://doi.org/10.1029/2021gl093462 (2021).
8. Arteaga, L. A., Behrenfeld, M. J., Boss, E. & Westberry, T. K. Vertical structure in phytoplankton growth and productivity inferred from biogeochemical-argo floats and the carbon-based productivity model. *Global Biogeochem. Cycles* **36**, 1–20 (2022).
9. Lacour, L., Llort, J., Briggs, N., Strutton, P. G. & Boyd, P. W. Seasonality of downward carbon export in the Pacific Southern Ocean revealed by multi-year robotic observations. *Nat. Commun.* **14**, 1–11 (2023).
10. Terrats, L. et al. BioGeoChemical-argo floats reveal stark latitudinal gradient in the southern ocean deep carbon flux driven by phytoplankton community composition. *Global Biogeochem. Cycl.* **37**, 1–28 (2023).
11. Vives, C. R., Schallenberg, C., Strutton, P. G. & Boyd, P. W. Biogeochemical-Argo floats show that chlorophyll increases before carbon in the high-latitude Southern Ocean spring bloom. *Limnol. Oceanogr. Lett.* **9**, 172–182 (2024).
12. Ryan-Keogh, T. J., Thomalla, S. J., Monteiro, P. M. S. & Tagliabue, A. Multidecadal trend of increasing iron stress in Southern Ocean phytoplankton. *Science (80-.)* **379**, 834–840 (2023).

13. Bock, N., Cornec, M., Claustre, H. & Duhamel, S. Biogeographical classification of the global ocean from BGC-argo floats. *Global Biogeochem. Cycles* **36**, 1–24 (2022).

14. Millie, D. F., Schofield, O. M., Dionigi, C. P. & Johnsen, P. B. Assessing noxious phytoplankton in aquaculture systems using bio-optical methodologies: a review. *J. World Aquac. Soc.* **26**, 329–345 (1995).

15. Roesler, C. S. & Barnard, A. H. Optical proxy for phytoplankton biomass in the absence of photophysiology: rethinking the absorption line height. *Methods Oceanogr.* **7**, 79–94 (2013).

16. Cullen, J. J. The deep chlorophyll maximum: comparing vertical profiles of chlorophyll a. *Can. J. Fish. Aquat. Sci.* https://doi.org/10.1139/f82-108 (1982).

17. Schallenberg, C. et al. Diel quenching of Southern Ocean phytoplankton fluorescence is related to iron limitation. *Biogeosciences* **17**, 793–812 (2020).

18. Roesler, C. et al. Recommendations for obtaining unbiased chlorophyll estimates from in situ chlorophyll fluorometers: a global analysis of WET Labs ECO sensors. *Limnol. Oceanogr. Methods* **15**, 572–585 (2017).

19. Falkowski, P. & Kiefer, D. A. Chlorophyll a fluorescence in phytoplankton: relationship to photosynthesis and biomass. *J. Plankton Res.* **7**, 715–731 (1985).

20. Claustre, H. et al. An intercomparison of HPLC phytoplankton pigment methods using in situ samples: application to remote sensing and database activities. *Mar. Chem.* **85**, 41–61 (2004).

21. Schmechtig, C., Poteau, A., Claustre, H., D'Ortenzio, F. & Boss, E. Processing Bio-Argo chlorophyll-a concentration at the DAC Level. *Argo Data Manag*. Version 1.0.30, 1–22 (2015).

22. Petit, F. et al. Influence of the phytoplankton community composition on the in situ fluorescence signal: implication for an improved estimation of the chlorophyll-a concentration from BioGeoChemical-Argo profiling floats. *Front. Mar. Sci.* **9**, 1–16 (2022).

23. Schallenberg, C., Strzepek, R. F., Bestley, S., Wojtasiewicz, B. & Trull, T. W. Iron limitation drives the globally extreme fluorescence/chlorophyll ratios of the Southern Ocean. *Geophys. Res. Lett*. **49**, (2022).

24. Xing, X. et al. Combined processing and mutual interpretation of radiometry and fluorimetry from autonomous profiling Bio-Argo floats: chlorophyll a retrieval. *J. Geophys. Res. Oceans* **116**, 1–14 (2011).

25. Morel, A. et al. Examining the consistency of products derived from various ocean color sensors in open ocean (Case 1) waters in the perspective of a multi-sensor approach. *Remote Sens. Environ.* **111**, 69–88 (2007).

26. Hu, C. et al. Improving satellite global chlorophyll a data products through algorithm refinement and data recovery. *J. Geophys. Res. Ocean.* **124**, 1524–1543 (2019).

27. O'Reilly, J. E. & Werdell, P. J. Chlorophyll algorithms for ocean color sensors—OC4, OC5 & OC6. *Remote Sens. Environ.* **229**, 32–47 (2019).

28. Schrader, P. S., Milligan, A. J. & Behrenfeld, M. J. Surplus photosynthetic antennae complexes underlie diagnostics of iron limitation in a cyanobacterium. *PLoS ONE* **6**, e18753 (2011).

29. Ryan-Keogh, T. J. & Thomalla, S. J. Deriving a proxy for iron limitation from chlorophyll fluorescence on buoyancy gliders. *Front. Mar. Sci.* **7**, 1–13 (2020).

30. Ryan-keogh, T. J. & Smith, W. O. Temporal patterns of iron limitation in the Ross Sea as determined from chlorophyll fluorescence. *J. Mar. Syst.* **215**, 103500 (2021).

31. Ustick, L. J. et al. Metagenomic analysis reveals global-scale patterns of ocean nutrient limitation. *Science (80-.)* **372**, 287–291 (2021).

32. Browning, T. J. & Moore, C. M. Global analysis of ocean phytoplankton nutrient limitation reveals high prevalence of co-limitation. *Nat. Commun.* **14**, 1–12 (2023).

33. Huot, Y. & Babin, M. Overview of fluorescence protocols: theory, basic concepts, and practice. In *Chlorophyll a Fluorescence in Aquatic Sciences: Methods and Applications* (eds. Suggett, D. J., Prášil, O. & Borowitzka, M. A.) (2010).

34. Babin, M., Morel, A. & Gentili, B. Remote sensing of sea surface sun-induced chlorophyll fluorescence: consequences of natural variations in the optical characteristics of phytoplankton and the quantum yield of chlorophyll a fluorescence. *Int. J. Remote Sens*. **17**, 2417–2448 (1996).

35. Johnson, K. S. et al. Biogeochemical sensor performance in the SOCCOM profiling float array. *J. Geophys. Res. Ocean.* **122**, 6416–6436 (2017).

36. Boss, E. S. & Haentjens, N. *Primer Regarding Measurements of Chlorophyll Fluorescence and the Backscattering Coefficient with WETLabs FLBB on Profiling Floats*. SOCCOM Technical Report 2016-1 (Princeton University, Princeton, NJ, 2016).

37. Ryan-Keogh, T. J. et al. Spatial and temporal drivers of fluorescence quantum yield variability in the Southern Ocean. *Limnol. Oceanogr.* **68**, 569–582 (2023).

38. Maritorena, S., Morel, A. & Gentili, B. Determination of the fluorescence quantum yield by oceanic phytoplankton in their natural habitat. *Appl. Opt.* **39**, 6725–6737 (2000).

39. Morrison, J. R. In situ determination of the quantum yield of phytoplankton chlorophyll a fluorescence: a simple algorithm, observations, and a model. *Limnol. Oceanogr.* **48**, 618–631 (2003).

40. Boyd, P. W. et al. The role of biota in the Southern Ocean carbon cycle. *Nat. Rev. Earth Environ.* **5**, 390–408 (2024).

41. Saba, V. S. et al. Challenges of modeling depth-integrated marine primary productivity over multiple decades: a case study at BATS and HOT. *Global Biogeochem. Cycl.* **24**, 1–21 (2010).

42. Xing, X. et al. Quenching correction for in vivo chlorophyll fluorescence acquired by autonomous platforms: a case study with instrumented elephant seals in the Kerguelen region (Southern Ocean). *Limnol. Oceanogr. Methods* **10**, 483–495 (2012).

43. Bisson, K. M. et al. Seasonal bias in global ocean color observations. *Appl. Opt.* **60**, 6978 (2021).

44. Szeto, M., Werdell, P. J., Moore, T. S. & Campbell, J. W. Are the world's oceans optically different? *J. Geophys. Res. Oceans* **116**, 1–14 (2011).

45. Johnson, R., Strutton, P. G., Wright, S. W., McMinn, A. & Meiners, K. M. Three improved satellite chlorophyll algorithms for the Southern Ocean. *J. Geophys. Res. Ocean.* **118**, 3694–3703 (2013).

46. Orsi, A. H., Whitworth, T. & Nowlin, W. D. On the meridional extent and fronts of the Antarctic Circumpolar Current. *Deep. Res. Part I* **42**, 641–673 (1995).

47. Fay, A. R. & McKinley, G. A. Global open-ocean biomes: mean and temporal variability. *Earth Syst. Sci. Data* **6**, 273–284 (2014).

48. Xing, X., Briggs, N., Boss, E. & Claustre, H. Improved correction for non-photochemical quenching of in situ chlorophyll fluorescence based on a synchronous irradiance profile. *Opt. Express* **26**, 24734–24751 (2018).

49. Sauzède, R., Johnson, J. E., Claustre, H., Camps-Valls, G. & Ruescas, A. B. Estimation of oceanic particulate organic carbon with machine learning. *ISPRS Ann. Photogramm. Remote Sens. Spat. Inf. Sci.* **V**, 949–957 (2020).

50. Schmechtig, C., Thierry, V. & The Bio-Argo Team. *Argo Quality Control Manual for Biogeochemical Data.* Argo Data Management 1–54 (LOV, Observatoire Océanologique, Bio-Argo Group, Villefranche-sur-Mer, France, 2016).

51. Dong, S., Sprintall, J., Gille, S. T. & Talley, L. Southern ocean mixed-layer depth from Argo float profiles. *J. Geophys. Res. Ocean.* **113**, 1–12 (2008).

52. Romanou, A., Rossow, W. B. & Chou, S. H. Decorrelation scales of high-resolution turbulent fluxes at the ocean surface and a method to fill in gaps in satellite data products. *J. Clim.* **19**, 3378–3393 (2006).

Author contributions

J.S.L. conceived the study, drafted the initial manuscript, and performed all data analysis with the exception of the autocorrelation analysis, which was performed by N.B., and the estimates of chlorophyll-a from radiometer data, which was performed by J.P. K.J. provided expert guidance on float characteristics and regional considerations that contributed to the final quality control of float data. All authors contributed to editing and improving the final manuscript with significant text added by Y.T. and A.J.F., both of whom greatly contributed to the interpretation and guidance in quality control processing of float data.

Competing interests

The authors declare no competing interests.

Additional information

Supplementary information The online version contains supplementary material available at https://doi.org/10.1038/s43247-024-01762-4.

Correspondence and requests for materials should be addressed to Jacqueline S. Long.

Peer review information *Communications Earth & Environment* thanks the anonymous reviewers for their contribution to the peer review of this work. Primary Handling Editors: Clare Davis and Alice Drinkwater. A peer review file is available

Reprints and permissions information is available at http://www.nature.com/reprints